Nuclear Inst. and Methods in Physics Research B 414 (2018) 113–120

Contents lists available at ScienceDirect

Nuclear Inst. and Methods in Physics Research B

journal homepage: www.elsevier.com/locate/nimb

Neutron flux and gamma dose measurement in the BNCT irradiation facility at the TRIGA reactor of the University of Pavia

S. Bortolussi[a,b,*], N. Protti[b], M. Ferrari[b,c], I. Postuma[b], S. Fatemi[a,b], M. Prata[b,d], F. Ballarini[a,b], M.P. Carante[a,b], R. Farias[e,f], S.J. González[e,f], M. Marrale[g,h,i], S. Gallo[j,k], A. Bartolotta[g,h], G. Iacoviello[l], D. Nigg[m], S. Altieri[a,b]

[a] Department of Physics, University of Pavia, via Bassi 6, 27100 Pavia, Italy
[b] Istituto Nazionale di Fisica Nucleare (INFN), Unit of Pavia, via Bassi 6, 27100 Pavia, Italy
[c] Department of Mechanical and Industrial Engineering, University of Brescia, via Branze 38, 25123 Brescia, Italy
[d] Laboratorio Energia Nucleare Applicata (LENA), University of Pavia, via Aselli 41, 27100 Pavia, Italy
[e] Comisión Nacional de Energía Atómica (CNEA), Av. De Los Constituyentes 1499, Buenos Aires, Argentina
[f] Consejo Nacional de Investigaciones CientÂficas y Técnicas (CONICET), Av. Godoy Cruz 2290, Buenos Aires, Argentina
[g] Department of Physics and Chemistry, University of Palermo, Viale delle Scienze Edificio 18, 90125 Palermo, Italy
[h] Istituto Nazionale di Fisica Nucleare (INFN), Unit of Catania, Via Santa Sofia, 64, 95123 Catania, Italy
[i] Advanced Technologies Network Center (ATeN Center), University of Palermo, Viale delle Scienze Edificio 18, 90125 Palermo, Italy
[j] Department of Physics, University of Milan, Via Giovanni Celoria, 16, 20133 Milano, Italy
[k] Istituto Nazionale di Fisica Nucleare (INFN), Unit of Milan, Via Giovanni Celoria, 16, 20133 Milano, Italy
[l] U.O.C.-Fisica Sanitaria A.R.N.A.S. Ospedale Civico Palermo, Italy
[m] Idaho National Laboratory, Idaho Falls, Idaho, USA

ARTICLE INFO

Keywords:
Neutron flux measurements
Neutron activation
Photon dosimetry
Alanine dosimetry
BNCT

ABSTRACT

University of Pavia is equipped with a TRIGA Mark II research nuclear reactor, operating at a maximum steady state power of 250 kW. It has been used for many years to support Boron Neutron Capture Therapy (BNCT) research. An irradiation facility was constructed inside the thermal column of the reactor to produce a sufficient thermal neutron flux with low epithermal and fast neutron components, and low gamma dose. In this irradiation position, the liver of two patients affected by hepatic metastases from colon carcinoma were irradiated after borated drug administration. The facility is currently used for cell cultures and small animal irradiation.

Measurements campaigns have been carried out, aimed at characterizing the neutron spectrum and the gamma dose component. The neutron spectrum has been measured by means of multifoil neutron activation spectrometry and a least squares unfolding algorithm; gamma dose was measured using alanine dosimeters.

Results show that in a reference position the thermal neutron flux is $(1.20 \pm 0.03) \times 10^{10}\,cm^{-2}\,s^{-1}$ when the reactor is working at the maximum power of 250 kW, with the epithermal and fast components, respectively, 2 and 3 orders of magnitude lower than the thermal component. The ratio of the gamma dose with respect to the thermal neutron fluence is 1.2×10^{-13} Gy/(n/cm^2).

1. Introduction

Boron Neutron Capture Therapy (BNCT) is an experimental radiotherapy based on the administration of a drug able to concentrate ^{10}B in tumour cells, followed by low energy neutron irradiation. Thermal neutron capture in ^{10}B generates two high LET particles (α and ^{7}Li ion) that lose all their energy in a range comparable to the cell diameter. In this short path, the charged particles cause irreparable damage to the cell where the reaction takes place, without directly affecting the surrounding healthy cells. Provided a sufficient boron concentration ratio between tumour and normal tissue, and a suitable neutron beam, the effect of the irradiation is selective at a cell level, delivering a lethal dose to the tumour while sparing the healthy tissues. Because of this characteristic, BNCT is a promising option to treat disseminated and infiltrated tumours that cannot be surgically removed nor treated with photon or hadron therapy [1].

In Pavia, BNCT has been tested as a therapy for whole organs (liver and lung) invaded by multiple metastases, and as an adjuvant treatment for tumours difficult to eradicate like osteosarcoma. The research started on liver, and led to a clinical application in two patients,

* Corresponding author at: Department of Physics, University of Pavia, via Bassi 6, 27100 Pavia, Italy.
E-mail address: silva.bortolussi@unipv.it (S. Bortolussi).

http://dx.doi.org/10.1016/j.nimb.2017.10.023
Received 18 May 2017; Received in revised form 20 October 2017; Accepted 23 October 2017

following the challenging protocol of ex-situ organ irradiation [2]. This application required the building of a proper irradiation position and its characterization in terms of neutron and photon dose components by experimental measurements and Monte Carlo simulations. The facility consists in an air channel ($40 \times 20 \times 100\ cm^3$) surrounded by graphite that ensures a good level of neutron thermalization. It is shielded with two bismuth walls that absorb the gamma radiation coming from the reactor core. The photon component is in fact a source of unwanted background dose in BNCT because it affects all the tissues in a non-selective way. A model of the whole reactor was produced using MCNP (version 4c2) [3] and the simulation results were validated with experimental measurements [4].

The facility is presently used to test the toxicity and the effectiveness of BNCT via *in vitro* and *in vivo* experiments. Moreover, a position in the thermal column is used to measure boron concentration in cell samples or tissues taken from animal models treated with new boronated formulations. In particular, the possibility to treat large portions of lung with external epithermal neutron beams has been explored, requiring the demonstration of the selective absorption of ^{10}B by lung tumour [5], and of BNCT effectiveness in an animal model. Monte Carlo calculations have been performed to design special shields for small animals (rats and mice) with windows for the tumour irradiation [6,7]. Animals are inserted in an air channel in the thermal column, at the same position where the liver had been irradiated, in order to keep the irradiation time as short as possible. In this second phase of BNCT research at the TRIGA reactor, new measurements and simulations have been carried out, with the goal of refining the dosimetry and producing proper treatment planning for animals.

This paper describes the measurements and the simulations performed in the recent years to characterize the dosimetry in the TRIGA thermal column, following an integrated approach based on neutron activation measurements, Monte Carlo simulation and alanine irradiation. Fig. 1 shows the MCNP5 geometry of the TRIGA reactor with the Thermal Column and the positions where the measurements were carried out.

The activation measurements performed were part of an international inter-comparison of thermal neutron facilities for samples and animal irradiations, comprising the MURR reactor in Missouri and the RA-3 reactor in Argentina [8]. The experiments and calculations were performed in collaboration with Idaho National Laboratory, where a protocol based on multi-foil neutron activation spectrometry and a least squares unfolding algorithm was developed for this specific purpose [9]. As the neutron field inside the thermal column has a broad energy spectrum, detectors with different behaviours of the cross section were used, in particular: “1/v materials” for the thermal range, resonance detectors for the epithermal range and a threshold detector for the fast component. Combining the information of the activation of each detector enabled the reconstruction of the neutron spectrum over the whole energy range, basing on a priori knowledge of the flux obtained by Monte Carlo simulation.

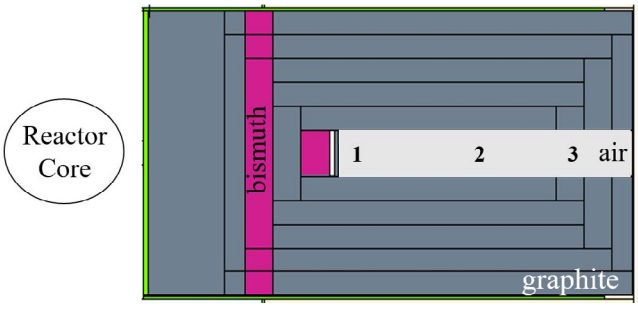

Fig. 1. Thermal column (longitudinal view) with the measurements positions. The neutron spectrum was measured in position 1 (130.95 cm from the centre of the core) while gamma doses were measured in positions 1, 2 (174.95 cm from the centre of the core) and 3 (208.95 cm from the centre of the core). Grey: graphite, magenta: bismuth, green: Boral (borated aluminium), white: air.

The alanine dosimetric system was mainly employed for gamma dose determination because of its valuable dosimetric features as passive radiation detector. In fact, ionizing radiations induce stable free radicals in the crystalline structure of the amino-acid L-α-alanine, quantitatively detectable via Electron Spin Resonance (ESR) technique [10]. These free radicals remain trapped in the matrix of alanine, with a very low fading (less than 1% per year in proper environmental conditions) [11]. Since the number of radicals generated is proportional to the delivered dose in a very wide range of energy, the amino-acid is widely employed as a passive solid-state dosimeter [12,13]. Photon tissue-equivalent composition, linear response in a very wide dose range (from around 1 to over 10^5 Gy), low dependence on the radiation quality, signal stability after irradiation, low dose-rate dependency, low cost and non-destructive readout (differently from thermoluminescence technique) are key advantages of alanine as dosimeter for photon and electron beams and for these properties alanine system was chosen for gamma dose determination [14–16].

Furthermore, ESR detectors response to different kinds of radiation was widely studied and recently an increasing interest has aroused toward neutrons and high LET charged particles [14,17–22,16,23, 15,24–37]. To compare the response of alanine to different radiation qualities and energies, the figure of merit considered is the Relative Effectiveness (RE) of an incident radiation with respect to ^{60}Co rays (with energies 1.173 and 1.333 MeV) in producing stable radicals. The RE is defined as the ratio of signals (S_{rad} and S_{Co}) after equal doses (D_{rad},D_{Co}) of reference radiation and radiation under investigation:

$$RE = \frac{S_{rad}}{S_{Co}} \quad \text{when} \quad D_{rad} = D_{Co}.$$

The energy dependence of RE for photon beams of different spectra, is experimentally demonstrated to be very low, while RE strongly depends on LET if the dose is deposited by charged particles. When energy is delivered by high-LET particles, the generated radicals are spatially more concentrated and can undergo recombination. The concentration of stable free radicals produced per ion generally decreases with decreasing of energy. Consequently, a decrease of RE is demonstrated to occur in correspondence of a LET increase over around 50 MeV/cm (5 keV/μm in water). Palmans [22] summarized the experimental RE measured in different experiments in the last 40 years for protons of energy between 1.2 and 60 MeV, fitting the curve of RE as a function of the effective energy of the proton beam (considering the effect of saturation) with a sigmoid. The sigmoid shows that for protons of energies between 0.6 MeV (protons generated from thermal neutron capture in nitrogen $^{14}N(n,p)^{14}C$ and 3.5 MeV (protons produced by elastic scattering of fast neutrons in hydrogen), RE is about 0.6. Schmitz et al. calculated that – for nitrogen protons – the RE value is 0.56 ± 0.01 [23] In the same paper, calculated RE values for the epithermal part of the spectrum are reported between 0.58 and 0.71 depending on the facility. The goal of this part of the work was to determine gamma dose in the thermal column, coupling alanine measurements to MC simulations. Alanine was shielded from thermal neutrons and an accurate MC model evaluated the neutron component still contributing to the dose absorbed by alanine. As a byproduct, the RE of all the dose components were evaluated by irradiating these dosimeters without any shielding in the thermal column at the TRIGA reactor in Pavia.

2. Materials and methods

2.1. The neutron spectrum measurements

First, a comprehensive analysis of the neutron spectrum was carried out. Three different set-ups were irradiated at the maximum reactor power of 250 kW: a set of bare foils, a set of foils under 1 mm thick Cd covers, and a foil under a thick ^{10}B shield. In particular: Au and Mn bare foils were irradiated for 10 min to measure the thermal component, In,

Table 1
List of the reactions considered for the multi-foil neutron irradiation campaign.

	Reaction	Energy range of primary response	Irradiation time
bare foils	^{55}Mn(n, γ)^{56}Mn ^{197}Au(n, γ)^{198}Au	Thermal Thermal	10 min
Cd-cover	^{115}In(n, γ)^{116}In	1 eV resonance	2 h
B sphere	^{197}Au(n, γ)^{198}Au ^{186}W(n, γ)^{187}W ^{55}Mn(n, γ)^{56}Mn ^{63}Cu(n, γ)^{64}Cu ^{115}In(n,n')^{115m}In	5 eV res. 18 eV res. 340 eV res. 1 keV res. > 0.3 MeV	6 h
Normalization	^{197}Au(n, γ)^{198} Au^{63}Cu(n, γ)^{64}Cu	–	

Au, W, Mn and Cu foils were irradiated under Cd for 2 h for the epithermal spectrum and a thick In foil was irradiated for 6 h inside a sintered hollow ^{10}B sphere to measure the fast range. The thin foils were positioned in a circular holder and placed inside the thermal column with a Teflon™ (Polytetrafluroethylene, PTFE) support and irradiated at Position 1 shown in Fig. 1 [38]. A detailed list of the reactions used and of the experimental conditions is reported in Table 1. Four Cu-Au wires were positioned in the 3 experiments at a fixed distance from the foils for normalization purposes. The foil and wires activities were measured using a standard high-purity Germanium gamma spectrometry system and the results were converted into saturation activities per atom to be used in the flux calculation.

The mathematical method used to extract the information about the neutron spectrum, consists in combining the experimental results and an *a priori* spectrum obtained by Monte Carlo calculation. The calculated spectrum is adjusted using the experimental values through an unfolding algorithm [9]. In particular, the reaction rate is expressed as the integral of the cross section ($\sigma_f(E)$), the *a priori* flux ($\Psi(E)$) and a self-shielding function ($P_f(E)$) that is the ratio of the perturbed (calculated in the foils, $\Psi_f(E)$) and unperturbed flux (calculated in the position of the foils but in absence of foils: *a priori*).

$$R = \int_0^\infty \sigma_f(E)\left(\frac{\Psi_f(E)}{\Psi(E)}\right)\Psi(E)dE = \int_0^\infty \sigma_f(E)P_f(E)\Psi(E)dE$$

By partitioning the range of energy into NG discrete contiguous energy group, the integral is turned into a summation, where a_j carries the information about the self-shielding function and the cross section:

$$R = \sum_{j=1}^{NG} a_j\phi_j$$

$$a_j = \frac{\int_{EL_j}^{EH_j} \sigma_f(E)P_f(E)\Psi(E)dE}{\int_{EL_j}^{EH_j} \Psi(E)dE}$$

$$\phi_j = \int_{EL_j}^{EH_j} \Psi(E)dE$$

where EL_j and EH_j are the lower and the upper energy limits of the jth energy group.

If NF different reactions are available in the experimental set-up, NF linearly independent equations can be written in matrix form as shown in Fig. 2; they can be also indicated in a more compact way as:

$$\mathbf{A\Phi = R}$$

where **A** is the sensitivity matrix, and Φ can be calculated by populating **R** with the measured reaction rates, under the assumption that the simulation for the evaluation of the *a priori* flux is accurate enough on a groupwise basis.

In case where $NF > NG$ the system is overdetermined and Φ is calculated by a least squares procedure using the so-called Normal Equations. In particular, the quantity to be minimized is the difference between the measured reaction rates and the expected ones:

$$\Delta = \sum_{i=1}^{NF} \frac{\delta_i^2}{u_i^2}$$

where u_i^2 is the experimental uncertainty and:

$$\delta_i = (R_i - (a_{i1}\phi_1 + a_{i2}\phi_2 + \cdots + a_{iNG}\phi_{NG}))$$

The mathematics lead to a new set of equations that can be expressed as:

$$\mathbf{A^T[Cov(R_m)]^{-1}A\Phi = A^T[Cov(R_m)]^{-1}R_m} \quad (1)$$

where $\mathbf{Cov(R_m)}$ is the $NF \times NF$ covariance matrix of the measured vector $\mathbf{R_m}$.

In this procedure, only the uncertainties affecting the measurements have been taken into account, but it is also possible to incorporate the *a priori* flux vector and its covariance, to provide further information. In this case, the measured reaction rates are substituted to **R** in the matrix of Fig. 2, but then the system is augmented as shown in Fig. 3, where $\phi_{01}, \phi_{02}, \ldots, \phi_{0NG}$ are the elements of the *a priori* calculated vector.

The vector Z is thus formed by the experimental reaction rates and the *a priori* flux vector. To arrive to an expression analogue to Equ. 1, the covariance matrix for the augmented vector Z is formed by the covariance matrix of the measured values ($Cov(R_m)$) and by the covariance matrix of the calculated flux values ($Cov(\Phi_0)$):

$$[Cov(Z)] = \begin{vmatrix} [Cov(R_m)] & [0] \\ [0] & [Cov(\Phi_0)] \end{vmatrix}$$

And the final adjusted vector Φ is obtained by solving the equation:

$$\mathbf{A^T[Cov(Z)]^{-1}A\Phi = A^T[Cov(Z)]^{-1}Z} \quad (2)$$

This latter approach is easily generalized to the underdetermined case as well, where the number of linearly independent measurements is lower than the number of groups desired in the adjusted spectrum and the necessary additional information is included in the a priori flux vector and its covariance.

2.2. The neutron spectrum simulations

In order to obtain the *a priori* flux vector in the most precise possible way, a Monte Carlo reactor model (MCNP, version 5 with the cross sections of the ENDF 6.0 library [39]) was produced. The entire geometry of the reactor with all its irradiation facility was already available, with a neutron/photon source obtained by criticality calculation (KCODE), modelling the fission reaction inside the fuel elements.

The geometry of each irradiation set-up was reproduced in two different modalities: modelling the holder and the foils with the corresponding materials (perturbed case) and replacing the materials with air (unperturbed *a priori* case). The first and second set-ups consisted in the Teflon holder containing the bare foils for thermal neutron component of the spectrum plus 4 copper wires, the second had the same geometries but different foils under Cd covers and the third consisted in the sintered boron sphere containing a thick indium foil. F4 tallies (neutron fluence) were calculated in the foils for each case, in 11 energy groups. Neutron fluence integrated with (n, γ cross sections were calculated coupling F4 with the tally multiplier FM to obtain the reaction rates in each foil. The same tallies were also calculated for the wires. The results were normalized to the operating power of the reactor (250 kW), which produces a source intensity of 1.6×10^{19} n/s.

Simulations were carried out in a multi-core cluster in order to reduce the calculation time. This was a critical point because the statistical convergence was slow, especially in the case of shielded foils (inside Cd covers or B sphere), and the results were not considered satisfying until all the energy bins had relative tally errors lower than

Multi-probe set
NG = energy intervals
NF= number of
measured reactions

$$\begin{bmatrix} a_{11} & a_{12} & a_{13} & \cdots & a_{1\,NG} \\ a_{21} & a_{22} & a_{23} & \cdots & a_{2\,NG} \\ a_{31} & a_{32} & a_{33} & \cdots & a_{3\,NG} \\ \vdots & \vdots & \vdots & & \vdots \\ \vdots & \vdots & \vdots & & \vdots \\ a_{NF\,1} & a_{NF\,2} & a_{NF\,3} & & a_{NF\,NG} \end{bmatrix} \begin{bmatrix} \phi_1 \\ \phi_2 \\ \phi_3 \\ \vdots \\ \phi_{NG} \end{bmatrix} = \begin{bmatrix} R_1 \\ R_2 \\ R_3 \\ \vdots \\ \vdots \\ R_{NF} \end{bmatrix}$$

Fig. 2. Matrix representation of the system to be solved in order to apply the unfolding algorithm.

5%. In order to make the simulations more efficient, special attention was dedicated to variance reduction. Weight windows were generated starting from an initial geometry splitting/Russian roulette play through several iterations, optimizing the tallies in the foils position.

The results were then coalesced to 4 groups to make the over-determined adjustment using the unfolding algorithm described above.

2.3. The gamma dose measurements and simulations

Alanine dosimeters were employed to measure the γ dose component in positions 1, 2 and 3 (Fig. 1) along the longitudinal axis of the thermal column.

For this work, EPR measurements were performed with commercial alanine pellets provided by Gamma-Service Produktbestrahlung GmbH. Pellets characteristics are: diameter 4.80 ± 0.04 mm, height 2.99 ± 0.02 mm, weight 68.0 ± 0.5 mg, density 1.26 ± 0.02 g/cm^3 and mass ratio alanine/binder 0.96/0.04. The radiation-induced free radicals in alanine are detected by using a Bruker ECS 106 spectrometer equipped with a TE_{102} rectangular cavity and operating in the X-band at approximately 9.70 GHz. The following parameters were set for EPR spectra acquisition: microwave power 6.32 mW, modulation amplitude 1 mT, modulation frequency 50 kHz, centre field 347 mT, field sweep width 30 mT. The sweep time (42 s), the time constant (655 ms) for 1024 points and the receiver gain were set in order to avoid any signal distortion. The first derivative of the EPR absorption spectrum was recorded at room temperature. The dosimeters were inserted in a Suprasil quartz tube with 5 mm internal diameter and centered inside the microwave cavity by means of Teflon spacers. The peak-to-peak amplitude of the central line was used as dosimetric parameter and was chosen in accordance with different authors [17,18]. As the EPR signal intensity could vary with orientation of the pellet inside the cavity, spectra were recorded at four different orientations with respect to the cylindrical axis of the tube. Three alanine pellets were used for each dose measurement. For each set of irradiation conditions (dose measurement), the mean value of 12 acquisitions of three dosimeters irradiated to the same configuration was calculated. The uncertainty of the EPR data for each irradiation setup and each dose value is the standard deviation of 12 measurements.

Since dose measurement were done in a mixed radiation field (neutrons and gamma), it was necessary to adopt some measures: one concerning the choice of the material to guarantee the electronic equilibrium, and another to separate the contributions of neutrons and gamma to the alanine response.

To ensure the necessary electronic equilibrium during the gamma dose measurements, alanine pellets were inserted in a graphite cylindrical holder of radius r = 2.1 cm and height h = 2.32 cm. Dosimeters were placed into the holders so that they were under 1 cm of graphite. Tissue-equivalent hydrogenated materials were avoided in order not to generate additional gamma dose due to the neutron capture in hydrogen, produced by the thermal neutron field present in the irradiation position. The other problem was that the gamma dose measurement was carried out in a mixed field where the thermal neutron component is predominant with respect to the gamma one. Alanine is very sensitive to thermal neutrons because it has a higher percentage of nitrogen than biological tissues. For this reason, alanine dosimeters were inserted into proper shields for thermal neutrons, made of 6-lithium carbonate (Li-6 enrichment: 95%), that attenuated the thermal neutron component of the flux by three orders of magnitude (Fig. 4) without producing additional gamma dose. For each position, also bare alanine was irradiated (unshielded configuration), to draw some conclusions on RE values for each dose components.

An important step of the experiment was the alanine dosimeters calibration. To choose the gamma source for calibration, a simulation of the gamma spectrum present in the irradiation positions was obtained with MCNP. Gamma spectrum in position 1 is shown in Fig. 5, where the peaks due to neutron capture in carbon and bismuth are clearly visible.

This type of spectrum makes Co-60 source not suitable for calibration, because it is only constituted by two peaks at 1.17 and 1.33 MeV. Instead, the irradiations of the alanine pellets were performed with 6

$$\begin{bmatrix} a_{11} & a_{12} & a_{13} & \cdots & \cdots & a_{1,\mathrm{NG}} \\ a_{21} & a_{22} & a_{23} & \cdots & \cdots & a_{2,\mathrm{NG}} \\ \vdots & \vdots & \vdots & & & \vdots \\ a_{\mathrm{NF},1} & a_{\mathrm{NF},2} & a_{\mathrm{NF},3} & \cdots & \cdots & a_{\mathrm{NF,NG}} \\ 1 & 0 & 0 & \cdots & \cdots & 0 \\ 0 & 1 & 0 & \cdots & \cdots & 0 \\ 0 & 0 & 1 & \cdots & \cdots & 0 \\ \vdots & \vdots & \vdots & & & \vdots \\ \vdots & \vdots & \vdots & & & \vdots \\ 0 & 0 & 0 & \cdots & \cdots & 1 \end{bmatrix} \cdot \begin{bmatrix} \varphi_1 \\ \varphi_2 \\ \varphi_3 \\ \vdots \\ \vdots \\ \varphi_{\mathrm{NG}} \end{bmatrix} = \begin{bmatrix} Rm_1 \\ Rm_2 \\ \vdots \\ Rm_{\mathrm{NF}} \\ \varphi_{01} \\ \varphi_{02} \\ \varphi_{03} \\ \vdots \\ \vdots \\ \varphi_{0\mathrm{NG}} \end{bmatrix} = [A][\Phi] = [Z]$$

Fig. 3. Matrix representation of the augmented system using the covariance matrix of the *a priori* flux.

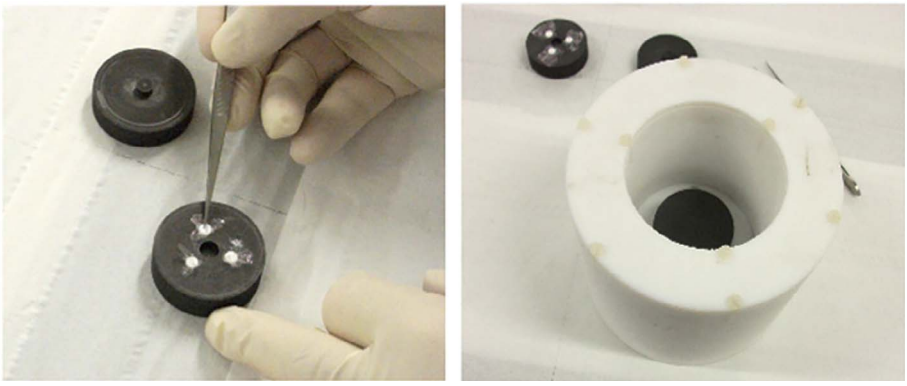

Fig. 4. Left: pictures of the experimental set-up: the alanine pellets are inserted into graphite holders to ensure the electronic equilibrium (left) and the holder is then inserted into a shield made of a Teflon container filled with 6-lithium carbonate to suppress the contribution of thermal neutrons to the total dose (right).

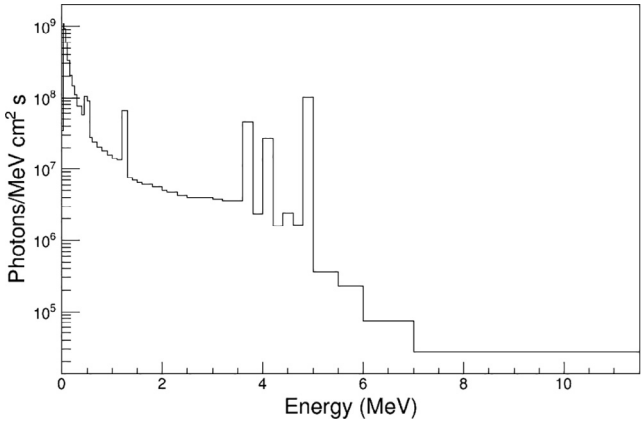

Fig. 5. Spectrum of the photon component in position 1, close to the reactor core, at the working power of 250 kW (see Fig. 1).

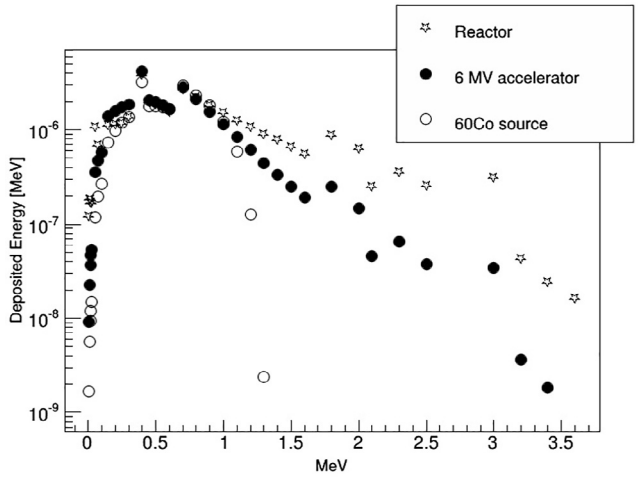

Fig. 6. Comparison between the spectra of the energy deposits in alanine due to the gamma spectrum present in the thermal column, to the 6 MV accelerator photon beam used for calibration, and to a standard ^{60}Co source.

MV X-ray beams generated by a medical linear accelerator (LINAC), a Siemens Primus (Siemens Medical Systems, CA, USA) at the radiotherapy department of A.R.N.A.S. Civico, Palermo (Italy). The LINAC was calibrated following the IAEA TRS-398 code of practice thus to obtain an equivalence of 1 cGy/1 Monitor Unit (MU) under reference conditions [40]. To validate this choice, we calculated the spectrum of the energy depositions in the dosimeters by secondary electrons in the case of linear accelerator and gamma background of the reactor thermal column (Fig. 6).

For calibration at 6 MV photon beam, the alanine pellets were placed in a graphite holder identical to the ones used for irradiation in the thermal column. A graphite cylinder of the same size of the dosimeter holders was built with a housing for a calibration ionization chamber (*Semiflex* type ionization chamber – 31010^{TM}, PTW: active volume 0.125 cm3, active length 0.65 cm), and was irradiated next to the holder with three alanine pellets.

The calibration was performed in graphite instead of water-equivalent material employed to calibrate the ionization chamber, and this required an adjustment of the dose read by the ionization chamber (previously calibrated in water), taking into account the ratio of the (μ_{en}/ρ) between water and graphite. The calibration thus obtained gave a relationship between the measured alanine signal S and the dose D absorbed by dosimeters, that was then used to convert the acquired data to dose values.

Finally, the whole irradiation set-up into the thermal column of the reactor was simulated with MCNP5 in order to separate the gamma component, the thermal neutron component, due to thermal neutron capture in nitrogen and hydrogen and the epithermal neutron scattering in hydrogen. Gamma dose calculation was carried out in two steps: first a gamma source was obtained in the thermal column by transporting neutrons and photons, then, this source was employed in a separate run, where the set-up was isolated from the rest of the reactor, tallying the dose in a coupled photon-electron transport.

3. Results

3.1. Neutron flux

The results of the MCNP neutron flux simulations in the irradiation position in an 11 energy group structure are plotted in Fig.7, representing the *a priori* spectrum used for the unfolding procedure.

Fig. 8 shows the comparison between the adjusted experimental spectrum (obtained by deconvolution of experimental measurements and *a priori* neutron flux values calculated by MCNP coalesced into 4 energy groups) and the *a priori* calculated spectrum. The agreement is good at least up to 10 keV, in fact, the energy range where the two curves are more different is the fast zone, where the neutron adjusted flux is almost a factor 3 lower than the *a priori* flux. Table 2 lists the comparison of the results.

3.2. Photon dose

The simulations provided the different components of the dose absorbed by alanine dosimeters: gamma dose, contribution of (n,p) reaction in nitrogen and of fast neutron scattering on hydrogen. Results are listed in Table 3 for the positions 1, 2 and 3.

From the values listed in Table 3, it is evident that the dose component due to thermal neutrons interacting with nitrogen through the (n,p) reaction is almost completely cut in the shielded mode, while the contribution due to the elastic scattering on hydrogen and gamma dose

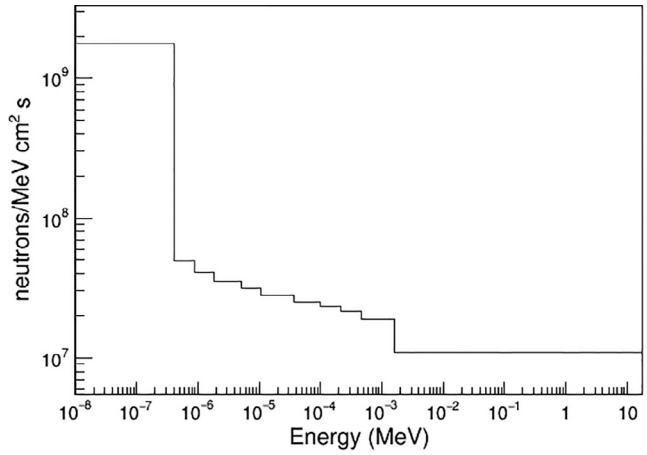

Fig. 7. A *a priori* spectrum calculated with MCNP5 over 11 energy bins in position 1, the simulation was normalized to a reactor power of 250 kW.

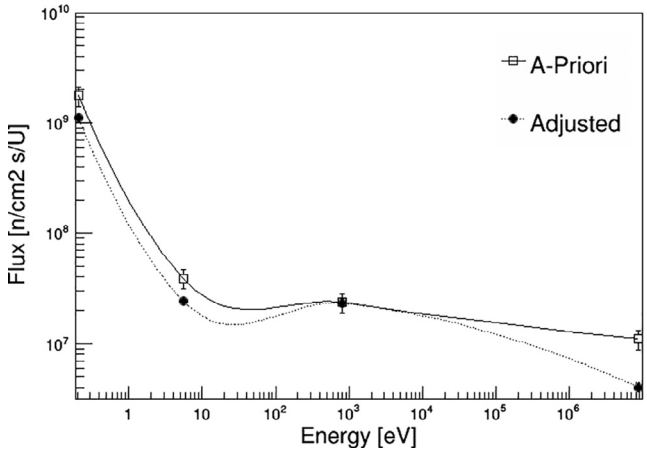

Fig. 8. Adjusted neutron spectrum (flux per unit lethargy) compared with the *a priori* spectrum calculated over 4 energy bins in position 1 when the reactor is working at the maximum power of 250 kW.

from background are almost the same in the two configurations. This demonstrates the effectiveness of the shield in eliminating the thermal neutron dose while not perturbing the gamma and fast neutron dose. Dose from neutrons of higher energy remains and it has to be properly weighted before comparing the simulation with the experimental results. An RE factor of 0.58 was chosen following the indications found in Schmitz et al. [23] to weight the fast neutron dose calculated in the shielded dosimeters. The values of the simulated weighted dose in the three positions is compared with the experimental results in Table 4.

The obtained values resulted in agreement with the experimental measurements within 2 standard deviations, thus the simulations were used to determine the gamma dose present in the irradiation positions. Table 5 reports the gamma dose rates in positions 1, 2 and 3.

In position 1, where the radiobiology experiments are carried out, the background gamma dose rate is about 5 Gy/h, the epithermal and fast neutron dose rate is about 2 Gy/h at the maximum reactor power. These dose values are contaminations that have an additional effect with respect to the dose due to thermal neutrons interacting with boron, nitrogen and hydrogen present in the sample or in the animal model. The measured thermal neutron flux unfolded with the *a priori* neutron spectra simulated with MCNP5 in this irradiation position is 1.2×10^{10} cm^{-2}s^{-1} when the reactor is working at 250 kW.

The results of the experiments and calculations in the unshielded

Table 3
Simulation of the dose components absorbed by alanine dosimeters in positions 1,2 and 3 of the thermal column when the reactor is working at the maximum power of 250 kW (Fig. 1). The components were calculated in two configurations: shielded in a lithium carbonate holder and bare. In order to calculate the gamma dose, the shielded results were used.

Dose component	Dose (Gy/h) Shielded	Dose (Gy/h) Unshielded
Position 1		
^{14}N(n,p)^{14}C	0.09 ± 0.03	68.6 ± 0.004
^{1}H(n,n')^{1}H	2.08 ± 0.05	2.42 ± 0.07
^{1}H(n, γ)^{2}H	–	0.38 ± 0.004
γbackground	5.34 ± 0.02	5.62 ± 0.006
Position 2		
^{14}N(n,p)^{14}C	0.05 ± 0.05	29.76 ± 0.004
^{1}H(n,n')^{1}H	0.45 ± 0.10	0.49 ± 0.12
^{1}H(n, γ)^{2}H	–	0.160 ± 0.004
γbackground	2.76 ± 0.02	2.900 ± 0.006
Position 3		
^{14}N(n,p)^{14}C	0.03 ± 0.05	16.590 ± 0.003
^{1}H(n,n')^{1}H	0.15 ± 0.1	0.19 ± 0.10
^{1}H(n, γ)^{2}H	–	0.090 ± 0.003
γ background	1.60 ± 0.03	1.72 ± 0.01

Table 4
Total (n + gamma) absorbed dose rates (Gy/h) in the shielded configuration when the reactor is working at the maximum power of 250 kW, in the 3 positions along the thermal column. RE = 0.58 for protons due to elastic scattering in H is used.

	Simulated	Measured
Pos.1	6.6 ± 0.2	6.0 ± 0.5
Pos.2	3.0 ± 0.1	2.6 ± 0.3
Pos.3	1.70 ± 0.05	1.51 ± 0.14

Table 5
Gamma dose rates in Gy/h in the 3 positions along the thermal column, obtained by MC simulations after proving that the calculated total dose is in agreement with experimental result. Dose values refer to the reactor working at 250 kW.

	Gamma dose (Gy/h)
Pos 1	5.3 ± 0.1
Pos 2	2.8 ± 0.1
Pos 3	1.6 ± 0.1

Table 2
The neutron flux at position 1 when the reactor is working at the maximum power of 250 kW (4 energy groups). Note that the Total σ associated with the *a priori* calculation is artificially increased so that the least-squares adjustment is primarily driven by the measurements and their covariances. MCNP5 calculations were run in order to obtain statistical uncertainties lower than 3% employing a cluster of CPUs and a set of weight windows separated by energy ranges of interest.

Energy range	Adjusted Flux (measurements unfolded with *a priori*flux calculations) (cm^{-2}s^{-1})	Total σ %	***A-Priori*** Flux (calculated by MCNP5 simulations) (cm^{-2}s^{-1})	Total σ %
< 0.414 eV	1.2E+10	2.5	1.8E+10	20.1
0.414E eV – 10.7 eV	7.9E+07	3.1	1.3E+08	20.1
10.7 eV – 1.58 keV	1.2E+08	6.1	1.2E+08	20.1
1.58 keV – 17.3 MeV	3.7E+07	11.5	1.0E+08	20.1

Table 6
Comparison of experimental values, the simulated components multiplied by RE = 0.58 and RE = 0.56 for the fast and thermal neutrons, respectively, and the simulated components multiplied by RE = 0.58 and RE = 0.4 for the fast and thermal neutrons, respectively. These values refer to the unshielded configuration and to the working power of 250 kW.

	Experimental alanine dose rate (Gy/h)	Simulated dose rate fast neutron * 0.58 thermal neutron * 0.56 (Gy/h)	Simulated dose rate fast neutron * 0.58 + thermal neutron * 0.4 (Gy/h)
Position 1	34.3 ± 2.3	45.8 ± 0.2	34.8 ± 0.1
Position 2	14.1 ± 1.1	20.01 ± 0.1	15.2 ± 0.1
Position 3	7.7 ± 0.5	11.2 ± 0.04	8.6 ± 0.03

configurations allowed further evaluation of the dosimeters behaviour. Without shield, the main contribution is due to thermal neutrons that must be added to the gamma and thermal neutron components after proper weighting by RE factor. The neutron dose components where firstly weighted using the RE values taken from literature (in particular, RE equal to 0.58 for fast neutron scattering on hydrogen and RE equal to 0.56 for thermal neutron capture in nitrogen). This first attempt led to an overestimation of the weighted sum of the calculated components if compared to the experimental results. However, based on the good agreement verified in the shielded case, and having validated the neutron transport in the reactor model, the dose components simulated in the unshielded configurations were used to propose a RE value for thermal neutrons to be applied in the thermal column of the TRIGA reactor in Pavia. It resulted that, for thermal neutron dose component, a RE value of 0.4 would be more suitable to reproduce experimental measurements. Table 6 reports the comparison of experimental values, the simulated components multiplied by RE = 0.58 and RE = 0.56 for the fast and thermal neutrons respectively, and multiplied by RE = 0.58 and RE = 0.4 for the fast and thermal neutrons, respectively. This finding is quite different from the value published to date [23]. Indeed, Schmitz et al. used a specific implemented user-routine of FLUKA code that is able to calculate the relative effectiveness of alanine for charged particles or neutrons by multiplying any energy deposition by a particle and energy specific RE, derived from the response model of Hansen and Olsen for the alanine detector [41]. Thanks to this routine they were able to simulate the the various contributions of the total dose in the mixed (n, γ) field of three reactors. Differently from the work of Schmitz et al. [23] whose major goal was to determine RE, in the present work alanine was employed to measure gamma dose suppressing the neutron components as much as possible by a ^{6}Li-carbonate shield. However, as the results were consistent with literature regarding the fast neutron, an additional step was made towards the determination of RE for thermal neutron capture in nitrogen. The obtained value of 0.4, lower than what published in the cited papers, suggests that further experiments and simulations are needed to confirm or modify these preliminary findings. Such deeper investigation is now under design.

4. Conclusions

This article presents a set of measurements performed in the thermal column of the TRIGA Mark II reactor of the University of Pavia with the aim of characterizing the neutron and the gamma components of the dose. The thermal column was originally modified to obtain an air channel for organ irradiation in a clinical trial of Boron Neutron Capture Therapy of explanted liver. Since then, the facility has been used for preclinical studies with small animal models and cell cultures. A simulation of the reactor was set-up, using MCNP5 with the neutron source based on criticality calculation. A method to measure the entire neutron spectrum in the animal irradiation position, consisting in an unfolding algorithm using both multi-foil activation results and *a priori* simulated values demonstrated that the new model is able to reproduce the neutron spectrum reliably at least up to 10 keV, which covers the large majority of the neutron flux in the facility. For gamma dose, a measurement campaign has been conducted with alanine dosimeters, using the same MCNP5 reactor model to separate the different dose components producing a signal in the detectors. Also in this case, the reactor model proved to be robust and suitable for treatment planning and dose evaluations, using the RE factor suggested by literature.

Presently, the thermal column of the TRIGA reactor operating in Pavia hosts a large irradiation facility (1 m by 40 cm by 20 cm) well characterized in terms of neutron spectrum and gamma dose, which can be used for different kinds of measurements requiring thermal neutron irradiation with flux values between 10^{9} and 10^{10} cm^{-2} s^{-1} and with low gamma contamination.

Acknowledgments

This work was sponsored in part by the Italian National Institute of Nuclear Physics (INFN), project NeTTuNO, in part by the Italian Ministry of Research and University (Project: “Development and application of new materials for ionizing radiation dosimetry”, P.I. F. d’Errico), and in part by the United States Department of Energy through the Idaho National Laboratory Faculty-Staff Exchange Program under DOE Idaho Operations Office Contract DE-AC07-05ID14517.

References

[1] R.F. Barth, M.H. Vicente, O.K. Harling, W. Kiger, K.J. Riley, P.J. Binns, F.M. Wagner, M. Suzuki, T. Aihara, I. Kato, et al., Current status of boron neutron capture therapy of high grade gliomas and recurrent head and neck cancer, Radiat. Oncol. 7 (1) (2012) 146.
[2] A. Zonta, U. Prati, L. Roveda, C. Ferrari, S. Zonta, A. Clerici, C. Zonta, T. Pinelli, F. Fossati, S. Altieri, et al., Clinical lessons from the first applications of BNCT on unresectable liver metastases., in: Journal of Physics: Conference Series, vol. 41, IOP Publishing, 2006, p. 484.
[3] J.F. Briesmeister, et al., MCNPTM-A general Monte Carlo N-particle transport code, Version 4C, LA-13709-M, Los Alamos National Laboratory (2000) 2.
[4] S. Bortolussi, S. Altieri, Thermal neutron irradiation field design for boron neutron capture therapy of human explanted liver, Med. Phys. 34 (12) (2007) 4700–4705.
[5] S. Bortolussi, J. Bakeine, F. Ballarini, P. Bruschi, M. Gadan, N. Protti, S. Stella, A. Clerici, C. Ferrari, L. Cansolino, et al., Boron uptake measurements in a rat model for Boron Neutron Capture Therapy of lung tumours, Appl. Radiat. Isot. 69 (2) (2011) 394–398.
[6] N. Protti, S. Bortolussi, S. Stella, M. Gadan, A. De Bari, F. Ballarini, P. Bruschi, C. Ferrari, A. Clerici, C. Zonta, et al., Calculations of dose distributions in the lungs of a rat model irradiated in the thermal column of the TRIGA reactor in Pavia, Appl. Radiat. Isot. 67 (7) (2009) S210–S213.
[7] D. Alberti, N. Protti, A. Toppino, A. Deagostino, S. Lanzardo, S. Bortolussi, S. Altieri, C. Voena, R. Chiarle, S.G. Crich, et al., A theranostic approach based on the use of a dual boron/Gd agent to improve the efficacy of boron neutron capture therapy in the lung cancer treatment, nanomedicine: nanotechnology, Biol. Med. 11 (3) (2015) 741–750.
[8] E.C. Pozzi, S. Thorp, J. Brockman, M. Miller, D.W. Nigg, M.F. Hawthorne, Intercalibration of physical neutron dosimetry for the RA-3 and MURR thermal neutron sources for BNCT small-animal research, Appl. Radiat. Isot. 69 (12) (2011) 1921–1923.
[9] S.R. Slattery, D.W. Nigg, J.D. Brockman, M.F. Hawthorne, Improved Computational Characterization of the Thermal Neutron Source for Neutron Capture Therapy Research at the University of Missouri, Tech. rep, Idaho National Laboratory (INL), 2010.
[10] D.F. Regulla, ESR spectrometry: a future-oriented tool for dosimetry and dating, Appl. Radiat. Isot. 62 (2) (2005) 117–127.
[11] E. Pauwels, H. De Cooman, M. Waroquier, E.O. Hole, E. Sagstuen, On the identity of the radiation-induced stable alanine radical, PCCP 12 (31) (2010) 8733–8736.
[12] W. Bradshaw, D. Cadena Jr, G. Crawford, H. Spetzler, The use of alanine as a solid dosimeter, Radiat. Res. 17 (1) (1962) 11–21.
[13] O. Baffa, A. Kinoshita, Clinical applications of alanine/electron spin resonance dosimetry, Radiat. Environ. Biophys. 53 (2) (2014) 233–240.
[14] J. Hansen, M. Waligorski, E. Byrski, Intercomparison of gamma ray, X ray, and fast neutron dosimetry using alanine detectors, Radiation Protection Dosimetry 27 (2) (1989) 85–92.
[15] M. Anton, L. Büermann, Relative response of the alanine dosimeter to medium energy x-rays, Phys. Med. Biol. 60 (15) (2015) 6113.
[16] M. Marrale, L. Abbene, F. d’Errico, S. Gallo, A. Longo, S. Panzeca, L. Tana, L. Tranchina, F. Principato, Characterization of the ESR response of alanine dosimeters to low-energy Cu-target X-tube photons, in press on Radiation Measurements, doi:http://dx.doi.org/10.1016/j.radmeas.2017.03.009.

[17] D. Regulla, U. Deffner, Dosimetry by ESR spectroscopy of alanine, Int. J. Appl. Radiat. Isot. 33 (11) (1982) 1101–1114.
[18] J. Arber, P. Sharpe, Fading characteristics of irradiated alanine pellets: the importance of pre-irradiation conditioning, Appl. Radiat. Isot. 44 (1–2) (1993) 19–22.
[19] M. Marrale, A. Carlino, S. Gallo, A. Longo, S. Panzeca, A. Bolsi, J. Hrbacek, T. Lomax, EPR/alanine dosimetry for two therapeutic proton beams, Nucl. Instrum. Methods Phys. Res., Sect. B 368 (2016) 96–102.
[20] M. Marrale, T. Schmitz, S. Gallo, G. Hampel, A. Longo, S. Panzeca, L. Tranchina, Comparison of EPR response of alanine and Gd 2 O 3-alanine dosimeters exposed to TRIGA Mainz reactor, Appl. Radiat. Isot. 106 (2015) 116–120.
[21] W. McLaughlin, ESR dosimetry, Radiat. Prot. Dosimetry. 47 (1–4) (1993) 255–262.
[22] H. Palmans, Effect of alanine energy response and phantom material on depth dose measurements in ocular proton beams, Technol. Cancer Res. Treat. 2 (6) (2003) 579–586.
[23] T. Schmitz, N. Bassler, M. Blaickner, M. Ziegner, M. Hsiao, Y. Liu, H. Koivunoro, I. Auterinen, T. Serén, P. Kotiluoto, et al., The alanine detector in BNCT dosimetry: dose response in thermal and epithermal neutron fields, Med. Phys. 42 (1) (2015) 400–411.
[24] M. Marrale, A. Longo, G. Russo, C. Casarino, G. Candiano, S. Gallo, A. Carlino, M. Brai, Dosimetry for electron Intra-Operative RadioTherapy: Comparison of output factors obtained through alanine/EPR pellets, ionization chamber and Monte Carlo-GEANT4 simulations for IORT mobile dedicate accelerator, Nucl. Instrum. Methods Phys. Res., Sect. B 358 (2015) 52–58.
[25] S. Onori, F. d'Errico, C. De Angelis, E. Egger, P. Fattibene, I. Janovsky, Alanine dosimetry of proton therapy beams, Med. Phys. 24 (3) (1997) 447–453.
[26] N. Bassler, J.W. Hansen, H. Palmans, M.H. Holzscheiter, S. Kovacevic, A.-A. Collaboration, et al., The antiproton depth–dose curve measured with alanine detectors, Nucl. Instrum. Methods Phys. Res., Sect. B 266 (6) (2008) 929–936.
[27] M. Marrale, M. Brai, G. Gennaro, A. Triolo, A. Bartolotta, Improvement of the LET sensitivity in ESR dosimetry for γ-photons and thermal neutrons through gadolinium addition, Radiat. Meas. 42 (6) (2007) 1217–1221.
[28] M. Marrale, A. Longo, S. Panzeca, S. Gallo, F. Principato, E. Tomarchio, A. Parlato, A. Buttafava, D. Dondi, A. Zeffiro, ESR response of phenol compounds for dosimetry of gamma photon beams, Nucl. Instrum. Methods Phys. Res., Sect. B 339 (2014) 15–19.
[29] M. Marrale, S. Basile, M. Brai, A. Longo, Monte Carlo simulation of the response of ESR dosimeters added with gadolinium exposed to thermal, epithermal and fast neutrons, Appl. Radiat. Isot. 67 (7) (2009) S186–S189.
[30] M. Marrale, A. Longo, M. D'Oca, A. Bartolotta, M. Brai, Watch glasses exposed to 6 MV photons and 10 MeV electrons analysed by means of ESR technique: A preliminary study, Radiat. Meas. 46 (9) (2011) 822–826.
[31] H. Gerstenberg, J. Hansen, J. Coyne, J. Zoetelief, Calculations of the relative effectiveness of alanine for neutrons with energies up to 17.1 mev, Radiat. Prot. Dosimetry. 31 (1–4) (1990) 85–89.
[32] A. Triolo, M. Marrale, M. Brai, Neutron–gamma mixed field measurements by means of MCP–TLD600 dosimeter pair, Nucl. Instrum. Methods Phys. Res., Sect. B 264 (1) (2007) 183–188.
[33] T. Schmitz, M. Blaickner, M. Ziegner, N. Bassler, C. Grunewald, J.V. Kratz, C. Schütz, P. Langguth, P. Sharpe, H. Palmans, et al., Dose determination using alanine detectors in a mixed neutron and gamma field for boron neutron capture therapy of liver malignancies, Acta Oncol. 50 (6) (2011) 817–822.
[34] T. Schmitz, M. Blaickner, C. Schütz, N. Wiehl, J.V. Kratz, N. Bassler, M.H. Holzscheiter, H. Palmans, P. Sharpe, G. Otto, et al., Dose calculation in biological samples in a mixed neutron-gamma field at the TRIGA reactor of the University of Mainz, Acta Oncol. 49 (7) (2010) 1165–1169.
[35] Y. Ikezoe, S. Sato, K. Onuki, N. Morishita, T. Nakamura, Y. Katsumura, Y. Tabata, Alanine dosimetry of 14 MeV neutrons in FNS target room, J. Nucl. Sci. Technol. 21 (9) (1984) 722–724.
[36] Y. Katsumura, Y. Tabata, T. Seguchi, N. Morishita, T. Kojima, Fast neutron irradiation effects–III. Sensitivity of alanine systems for fast neutron having an energy of ca 1 MeV, International Journal of Radiation Applications and Instrumentation. Part C, Radiat. Phys. Chem. 28 (4) (1986) 337–341.
[37] H. Schraube, E. Weitzenegger, A. Wieser, D. Regulla, Fast neutron response of alanine probes, Int. J. Radiat. Appl. Instrum. Part A 40 (10–12) (1989) 941–944.
[38] N. Protti, S. Bortolussi, M. Prata, P. Bruschi, S. Altieri, D.W. Nigg, Neutron spectrometry for the University of Pavia TRIGA? thermal neutron source facility, Trans. Am. Nucl. Soc. 107 (2012) 1269.
[39] J.S. Hendricks, MCNPX version 2.5. c, Tech. rep., Los Alamos National Laboratory, 2003.
[40] P. Andreo, M.S. Huq, M. Westermark, H. Song, A. Tilikidis, L. DeWerd, K. Shortt, Protocols for the dosimetry of high-energy photon and electron beams: a comparison of the IAEA TRS-398 and previous international Codes of Practice, Phys. Med. Biol. 47 (17) (2002) 3033.
[41] J.-W. Hansen, K. Olsen, Theoretical and experimental radiation effectiveness of the free radical dosimeter alanine to irradiation with heavy charged particles, Radiat. Res. 104 (1) (1985) 15–27.